

SUPPLEMENTARY INFORMATION

Figure S1 ChIP analyses of H4 acetylation at the telomere of the right arm of the chromosome VI.

(A) Schematic of Telomere VI R. TG₁₋₃: Terminal stretch of telomeric repeats on the right arm of Chromosome VI. XC: Telomeric X element, Core sequence containing an ARS consensus sequence and an Abf1p binding site. The thick black line (TEL) represents the subtelomeric region amplified in the ChIP experiments (0,6 Kb from the telomere right end).

(B) Global H4 acetylation at the telomere VI R of the specified strains. Cells were grown to log phase and chromatin was immunoprecipitated with antibodies against the C-terminal tail of histone H4 (H4 C-TERM) or against H4 acetylated at lysines 5, 8, 12 and 16 (ACH4). PCR was performed with primer sets for TEL and the ACT1 coding region as loading control. IP/INPUT ratio was calculated after normalization of TEL signals to the ACT1 control. In the graphs acetylation data were normalized to the total H4 occupancy and given as [mutant or treatment/wild-type] ratios (see Materials and Methods).

Mutation of SIR2 gene and NAM treatment lead to an increase in histone H4 acetylation, as expected (Braunstein et al., 1996) while the *rpd3* mutant shows a two fold reduction in H4 acetylation. The remaining mutations analyzed (*hst1-4*, *nhp6ab*), do not have any effect on the amount of H4 acetylation.

(C) Acetylation level of histone H4 lysine 16 in the specified mutants. Same as in (B) but the antibodies were anti acetyl Histone H4-lysine 16 (H4K16-ac) and anti H4 C-terminal tail (H4 C-TERM). *sir2* mutants and NAM treated cells show an increase in histone H4K16 acetylation relative to WT, as expected (Braunstein et al., 1996; Ehrentraut et al., 2010) while the *RPD3* deletion lead to a two fold reduction in the acetylation content. Mutations in the sirtuins coding genes (*hst1-4*), have no effect on the level of H4K16 acetylation. The telomere of the *nhp6ab* mutant appears to have a slight decrease in the level of H4K16 acetylation.

Figure S2 ChIP analyses of H4K12 and H3K56 acetylation at the rDNA and telomere VI R of *rpd3* and *hst3* mutants.

(A) H4K12 acetylation profile at the rDNA and at the telomere VI R of the *rpd3* mutant. Chromatin extracts derived from WT and *rpd3* cells were immunoprecipitated with antibodies against the C-terminal tail of histone H4 (H4 C-TERM) or anti acetyl histone H4-lysines 12 (H4K12-ac). The regions analyzed were the rDNA repeat (left) and the telomere VI R (right). See Figure 4 and Figure S1 for the positions of PCR amplicons and quantification methods. The *rpd3* mutant shows a slight decrease in H4K12 acetylation at rDNA, without changes in the acetylation level at telomere.

(B) H3K56 acetylation profile at the rDNA and at the telomere VI R of the *hst3* mutant. Same as in (A) but the chromatin extracts were from WT and *hst3* cells and the antibodies used were anti H3 C-terminal and anti acetyl histone H3-lysines 56 (H3K56-ac). rDNA of the *hst3* mutant is slightly hyperacetylated relative to the WT level of acetylation. No change was found at telomere.

Figure S3 Sir2p recruitment at rDNA is not impaired in *rpd3* and *hst3* mutants.

Sir2p binding at the rDNA of *rpd3* (A) and *hst3* (B) mutants.

Mutant cells were analyzed, with the corresponding isogenic WT strains, by ChIP with antibodies against Sir2p. Sir2p enrichment was calculated at two rDNA regions, ENH and C-PRO, as described in Figure 7 and in Materials and Methods. No significant change in the binding of Sir2p has been found at the rDNA of the *rpd3Δ* and *hst3Δ* strains, relative to the WT.

Figure S4 Effects of the *nhp6ab* mutation on Sir2p recruitment at telomere VI and on subtelomeric gene expression.

(A) Sir2p binding at the telomere of the right arm of Chromosome VI slightly decrease in the *nhp6ab* mutant. WT and *nhp6ab* chromatin extract were immunoprecipitated with anti Sir2

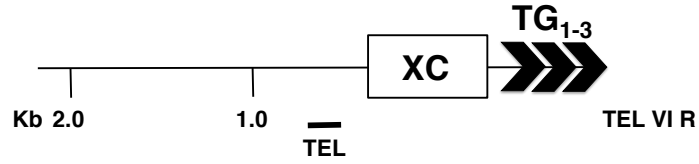
antibodies. The region amplified in the PCR reaction is 0,6 Kb from the telomere right end (see Figure S1 for position). IP/input ratios, normalized to the ACT1 control, are shown.

(B) The *nhp6ab* double mutation does not affect the expression of subtelomeric genes.

The upper part of the figure shows the ORFs located at the telomere VI R and their distance from the telomere end. The expression level of YFR057W and IRC7 in WT and *nhp6ab* strains was analyzed by RT-PCR. In the graph the transcription levels of the two genes are given as fold enrichment relative to ACT1.

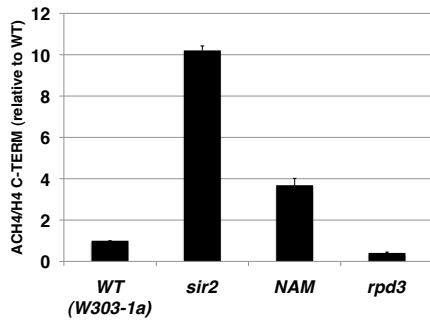
Figure S1

A



B

ACH4



C

H4K16-ac

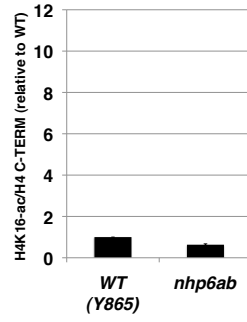
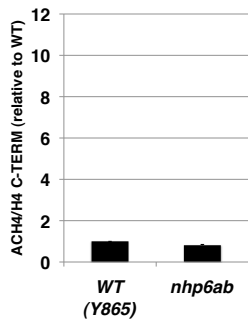
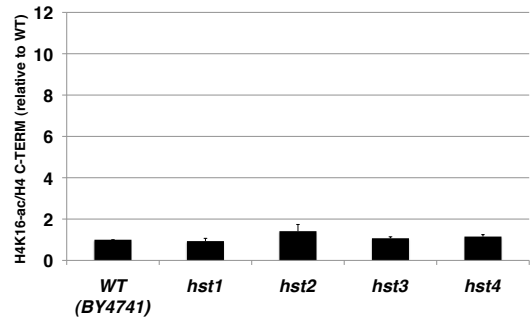
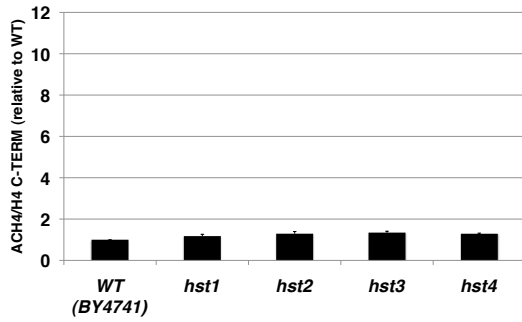
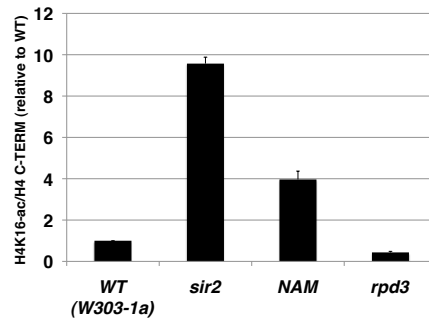


Figure S2

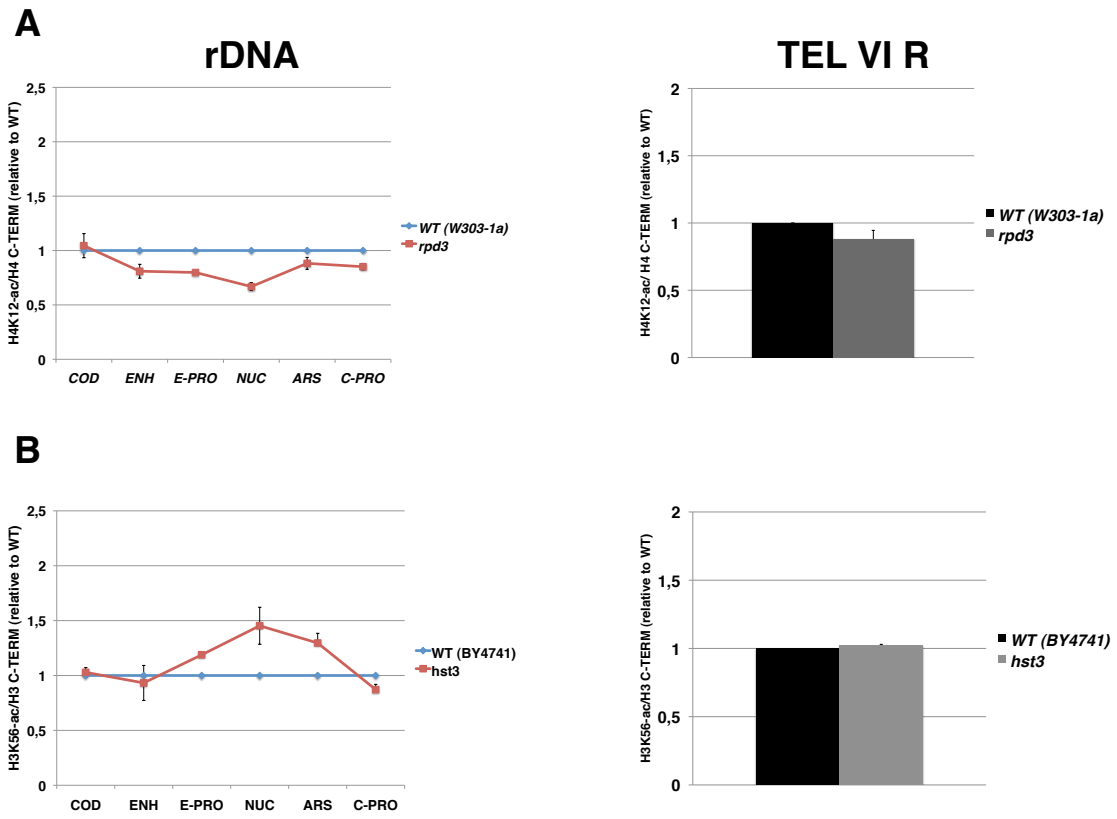


Figure S3

A



B

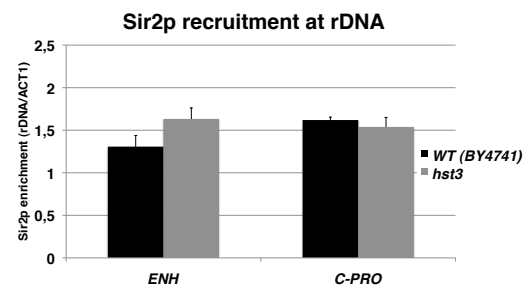
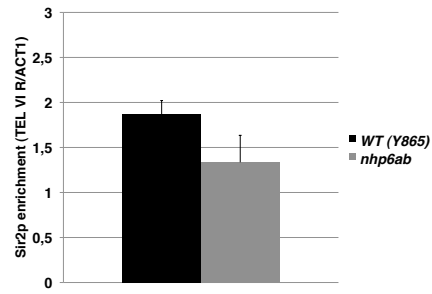


Figure S4

A



B

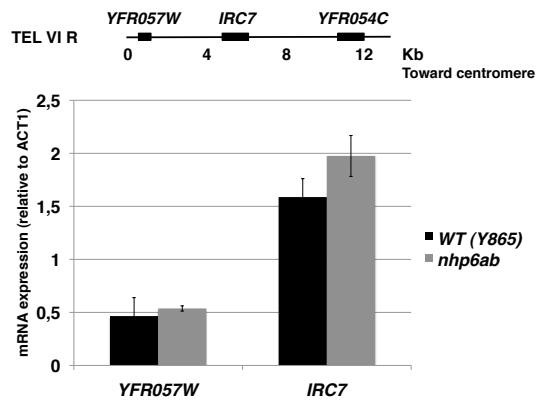


Table S1 Yeast strains and plasmids used in this study

<i>Strain</i>	<i>Genotype</i>	<i>Background (source)</i>
WT	<i>MATa; ade2-1; ura3-1; his3^{11,15}; trp1-1; leu2-3,112; can1-100</i>	W303-1a
<i>sir2</i>	<i>MATa; ade2-1; ura3-1; his3-11,15; trp1-1; leu2-3,112; can1-100; sir2::LEU2</i>	W303-1a (NOY1045, kindly provided by M. Nomura)
<i>rpd3</i>	<i>MATa; ade2-1; ura3-1; his3-11,15; trp1-1; leu2-3,112; can1-100; rpd3::LEU2</i>	W303-1a (WJY140, kindly provided by M. Grunstein)
WT	<i>MATa; his3-Δ1; leu2-Δ0; met15-Δ0; ura3-Δ0</i>	BY4741 (from Invitrogen, Grand Island, New York, USA)
<i>hst1</i>	<i>MATa; his3-Δ1; leu2-Δ0; met15-Δ0; ura3-Δ0; hst1::KAN</i>	BY4741 (BY1760, from Invitrogen)
<i>hst2</i>	<i>MATa; his3-Δ1; leu2-Δ0; met15-Δ0; ura3-Δ0; hst2::KAN</i>	BY4741 (BY2813, from Invitrogen)
<i>hst3</i>	<i>MATa; his3-Δ1; leu2-Δ0; met15-Δ0; ura3-Δ0; hst3::KAN</i>	BY4741 (BY1801, from Invitrogen)
<i>hst4</i>	<i>MATa; his3-Δ1; leu2-Δ0; met15-Δ0; ura3-Δ0; hst4::KAN</i>	BY4741 (BY3550, from Invitrogen)
WT	<i>MATα; ura3-52; trp1-289; his3-Δ1; leu2-3,112; gal 2; gal 10</i>	Y865 (kindly provided by M.E. Bianchi)
<i>nhp6ab</i>	<i>MATα; ura3-52; trp1-289; his3-Δ1; leu2-3,112; gal 2; gal 10; nhp6a-Δ3::URA3; nhp6b-Δ3::HIS3</i>	Y865 (Y869, kindly provided by M.E. Bianchi)
WT	<i>MATa, ade2-101, his3-D200, leu2-3,-112, lys2-801, trp1-</i>	<i>PKY501</i> (kindly provided by M. Grunstein)

	<i>D901, ura3-52, thr tyr arg4-1, hhf1::HIS3; hhf2::HIS4/ pPK301 (CEN3, ARS1, URA3, HHF2)</i>	
H4K16Q	<i>MATa, ade2-101, his3-D200, leu2-3,-112, lys2-801, trp1-D901, ura3-52, thr tyr arg4-1, hhf1::HIS3; hhf2::HIS4/ pLJ912(CEN3, ARS1, URA3, hhf2 K16Q)</i>	<i>PKY501</i> (LJY912, kindly provided by M. Grunstein)
WT	<i>MATa HMRA-e** hht1-hhf1D::LEU2 hht2-hhf2D::HIS3 pRS414-[HHT1-HHF1]</i>	AEY1558 (kindly provided by A. E. Ehrenhofer-Murray)
H4K16R	<i>MATa HMRA-e** hht1-hhf1D::LEU2 hht2-hhf2D::HIS3 pRS414-[HHT1-hhf1-21 (K16R)]</i>	AEY1558 (AEY1956, kindly provided by A. E. Ehrenhofer-Murray)
<i>Plasmid</i>	<i>Features</i>	<i>Reference</i>
pAR44	2 μ , <i>TRP1</i> , <i>GAL10</i> promoter, <i>SIR2</i>	Holmes et al., 1997
pGC102	2 μ , <i>TRP1</i>	pGBKT7 (Clontech)

Table S2 Oligonucleotides used in this study

<i>Oligonucleotide</i>	<i>Oligonucleotide sequence (in 5' to 3' direction)</i>
NTS1-Rf	GCACCATCAGAGCGGCAAAC
NTS1-Rr	CGCTGCCTCTCTGGAAC
ACT1-F	AGTCAGTCAAATCTCTACCGGCCA
ACT1-R	ACGTTCCAGCCTTCTACGTTTCCA
SIR2-F	ACGCGATCAGAAAACAACCCGATG
SIR2-R	CTTGGGCGTCTCTGGTTTCAAAC
YFR057W-F	CTATAGTAAGTGCTCGGCCAAGTC
YFR057W-R	CTCTTCTGAGACGAAGTCGTTGCT
IRC7-F	CAACCGTCATTTTCCTCGAAAGCC
IRC7-R	GCAATGCTAATTGACAGTCCTCGG
COD-F	GGGCTCATGGA GAACAGAAATCTC
COD-R	CCGAATGAACTGTTCCCTCTCGTAC
ENH-F	GGGGCCTAGTTTAGAGAGAAGTAG
ENH-R	CTCTGATGGTGCGGAAAAAACTGC
E-PRO-F	TGTTAGTGCAGGGAAAGCGGGAAGGA
E-PRO-R	GCACTATCCAGCTGCACTCTTCTTC
NUC-F	ATGTTTCAGTAGGTGGGAGTGAGAG
NUC-R	CATCCGGTGCCGTAAT GCAAAAC
ARS-F	AAAGTGGACAGAGGAAAAAGGTGCG
ARS-R	GTGACGGAAATACGCTTCAGAGAC
C-PRO-F	AATAGTGAGGAACTGGGTTACCCG
C-PRO-R	TTGTACTCCATGACTAAACCCCC
TEL VI-F	GCGTAACAAAGCCATAATGCCTCC
TEL VI-R	CTCGTTAGGATCACGTTTGAATCC